Harnessing the potential of lead-free Sn-Ge based perovskite solar cells by unlocking the recombination channels

Yassine Raoui,[a,c] Samrana Kazim,[a,b*] Yulia Galagan,[d] Hamid Ez-Zahraouy[c] and Shahzada Ahmad[*a,b]

Perovskite solar cells (PSCs) have celebrated a decade of investigation as a promising photovoltaic technology. However, they contain lead, inorganic lead-free PSCs can be designed as green and clean energy sources. To overcome the current obstacles in lead-free PSCs, the stability and performance gap should be minimized. The Drift-Diffusion simulation model is a conducive way to understand the working mechanism in a thin-film solar cell. Here we adopted a computational approach to design and investigate the performance of $CsSn_{0.5}Ge_{0.5}I_3$ as a light harvester. We optimize the thickness of perovskite, for its use in inverter planer structure (FTO/PCBM/$CsSn_{0.5}Ge_{0.5}I_3$/Spiro-OMeTAD/Au). Furthermore, cerium oxide (CeO_x) and PTAA are used as an alternative electron and hole transport layer, respectively. We studied the effect of trap density in the bulk $CsSn_{0.5}Ge_{0.5}I_3$ and its impact on performance, recombination rate, and diffusion length. The open-circuit voltage (V_{oc}) showed a significant improvement and the correlation with the trap density at the interface layers is established. We noted that the defect density at the perovskite/hole selective layer interface has a profound impact on the performance of lead-free-PSCs as compared to the electron selective layer/perovskite interface. By optimizing defects parameters it can deliver a PCE of 24.20%, V_{oc} = 1.17V, J_{sc} = 25.80 mA/cm^{2,} and FF = 80.33 %. Our findings provide access guidelines and pave the way for lead-free PSCs based on the Sn-Ge combination to approach their limit.

1. Introduction

Perovskite solar cells (PSCs) established themselves as a "rising star" in thin-film photovoltaic (PV) technologies. The Pb-based PSCs are attracting enormous attention due to their unparalleled electro-optical properties that led to record performance in thin-film PV. [1–3] However, the toxicity of lead is considered as an impermeable barrier to its success. According to the Goldschmidt tolerance factor, an effective perovskite absorber layer should have a value between 0.8 – 1.0. Tin (Sn) and Germanium (Ge) are ideally suited to replace Pb to form a perovskite structure and display higher optical absorption coefficients as compared to Pb. However, due to the low chemical stability of Sn^{2+} and Ge^{2+}, fewer studies have been reported. Nevertheless, due to the low optical band gaps and high charge carrier mobilities, Sn-based perovskite are the preferred choice of the PSCs research community. Organic-inorganic Sn-based PSCs were developed,[4] followed by numerous efforts to improve the performance of Sn-based PSCs.[5–9] However, thermal durability at high temperature, due to the volatile nature of organic elements is a challenge for organic-inorganic Sn-based PSCs. [10] On the other hand, all-inorganic $CsBI_3$ is one of the promising materials of Sn-based PSCs, where the B site is either Sn or Ge. By employing the Sn, binary structures are formed which could be suitable for solar application, β-γ-$CsSnI_3$ a black orthorhombic phase, and yellow γ-$CsSnI_3$ phase.[11,12] β-γ-$CsSnI_3$ exhibits a bandgap of ~1.3 eV, which is near to the ideal value (1.34 eV). [13] Besides, $CsSnI_3$ offers low toxicity and high thermal (450 °C) stability.[14] $CsSnI_3$ can be easily converted to the yellow orthorhombic phase (Pnma, γ) at room temperature upon exposure to air, oxygen, or water vapor.[12] Sn-based perovskite undergoes self-doping through oxidation (Sn^{2+} to Sn^{4+}), which in turn increases the hole density and led to short circuit or low-performance PCE, limiting the power conversion efficiency (PCE) to 4.81 %. [15] The use of additives such as SnF_2, $SnCl_2$, and excess SnI_2 can retard the generation of tin vacancies by neutralizing the traps. [15–17] Moreover, organic additives were also applied, such as piperazine or hydroxybenzene sulfonic acids to improve the PCE and stability. [18,19] The competitive performance of tin-germanium alloy ($CsSn_{0.5}Ge_{0.5}I_3$), with an optical band gap of 1.5 eV, gave a PCE of 7.11 % with the stability of over 500h under continuous operations. The fabrication of PSC was based on the solid-state reaction between mixed powder precursor CsI: SnI_2:GeI_2 carried out in evacuated Pyrex tubes with the PCBM and Spiro-OMeTAD as electron transport layer (ETL) and hole transport layer (HTL), respectively.[20] The competitive results demonstrated a new pathway to fabricate lead-free PSCs and the impact of interface passivation on the performance of PSCs. Despite such advancement, the performance remains lower as compared to the theoretical values. The stability of PCBM and Spiro-OMeTAD is still unclear. [21,22] As an alternative, cerium oxide (CeO_x), can be applied as ETL and can be processed at low temperature (<150 °C), [23,24] it shows a wide bandgap, high thermal and chemical stability, and high ionic conductivity. [25–28] Polytriarylamine (PTAA) is a promising HTL to fabricate efficient PSCs.[29,30] We can assume that the low performance reported with $CsSn_{0.5}Ge_{0.5}I_3$ based PSCs could be related to the nature of the selective layer and the high recombination in the bulk perovskite or at the interfacial layers. [31,32] Zhenyi et al [33] demonstrated the distribution and impact of trap densities in bulk perovskite layer and its interfaces on the performance of inverted PSCs using drive-level capacitance profiling (DLCP) and Drift-diffusion simulation. The priority of reducing the trap-assisted density either at the perovskite/HTL or the ETL/perovskite interfaces should be clarified as well. The non-radiative recombination is dominant in PSCs, occurring either at the grain boundaries or perovskite/HTL and ETL/perovskite and it is governed by trap-assisted recombination. [34] A recent report suggests, the synergetic problems of Sn-Ge need to be solved by finding an effective approach to improve the voltage and PV properties.

Thus, charge selective materials, the trap density in the bulk of perovskite, and its interfaces need to be engineered to boost the performance of Sn-Ge-based PSCs.[35,36] The macroscopic simulation such as the Drift Diffusion model can be an effective approach to overcome this challenge without sacrificing laboratory consumables, manpower, and less time to cut down the cost.[37–39]

Herein, to figure out the performance limit of using $CsSn_{0.5}Ge_{0.5}I_3$ as an absorber layer, we computed the *n-i-p* structure i.e., FTO/PCBM/$CsSn_{0.5}Ge_{0.5}I_3$/Spiro-OMeTAD/Au by employing the Solar Capacitor Simulator (SCAPS), the first simulation model was compared to the experimental studies reported. We optimized the thickness of the absorber layer by following the performance improvement. Additionally, we employed CeO_x and PTAA as ETL and HTL as charge selective layers. Subsequently, the effect of defect density (N_t) in the absorber layer and ETL/perovskite and perovskite /HTL were studied.

2. Device simulation parameters

The simulations were performed using the one-dimensional Solar cell capacitance simulator SCAPS 3.3.07 software [37] based on the Poisson equation and the continuity equations for electrons and holes.

$$\frac{d}{dx}\left(\varepsilon(x)\frac{d\Psi}{dx}\right) = q[\,p(x) - n(x) + N_D^+(x) - N_A^-(x) + p_t(x) - n_t(x)\,] \quad (1)$$

$$\frac{1}{j}\frac{\mathrm{d}J_p}{\mathrm{d}x} + R_p(x) - G(x) = 0 \quad (2)$$

$$-\frac{1}{j}\frac{\mathrm{d}J_n}{\mathrm{d}x} + R_n(x) - G(x) = 0 \quad (3)$$

Here, ε the permittivity and q the charge of the electron, Ψ is the electrostatic potential and *n* the free electrons, p free holes, n_t trapped electrons, p_t trapped holes, N_{D+} the ionized donor-like doping and N_{A-} the ionized acceptor-like doping concentrations, Rn(x), Rp(x) are electrons and holes recombination rate, G(x) is the generation rate, Jn and Jp are, respectively, the electron and hole current densities.

The adopted device architecture for simulated planar PSCs was FTO/PCBM/interface layer 1(IL1) /$CsSn_{0.5}Ge_{0.5}I_3$/interface layer2 (IL2)/ Spiro-OMeTAD /Au. Firstly, the defect density (N_t) of the absorber layer, [20] which measures the quality of the crystal, is set to be 1E16 cm^{-3} and is considered neutral, and capture cross-section of electron and hole is 1×10^{-14} cm^2. The electron and hole thermal velocity is 10^7cm/s. Taking into account interface recombination, two ultra-thin layers at ETM/Absorber (IL1) and Absorber/HTM (IL2) with an initial defect density of 1E18 cm^{-3} were inserted. The other parameters for each layer are shown in Table 1, where N_A and N_D denote acceptor and donor densities, ε_r is relative permittivity, χ is electron affinity, E_g is the bandgap energy, μ_n and μ_p are mobilities of electron and hole, and N_t is defect density. The Pre-factor A_α is set to 10^5 to obtain absorption coefficient (α) by $\alpha = A_\alpha(h\nu E_g)^{1/2}$. Metallic gold (Au) is used as the back and fluorine-doped tin oxide (FTO) as the front contact. The simulations were carried out at AM 1.5G illumination.

3. Results and discussion

The performance of our first model is close to the experimental values recently reported. [20] We adopted our first model by selecting simulation inputs from the experimental literature before further optimization. The thickness of the perovskite layer was kept to 200 nm, and it was deduced from the experimental report suggesting the best performance. Arguably, improving this value will be the first route to enhance the absorption and increase the external quantum efficiency (EQE). Another channel can be the source of recombination ($\boldsymbol{R'}$), stemming from the mismatch energy level between the light harvester and charge selective layers, which can be described as:

$$R' = CBO + VBO \quad (1)$$

The CBO is the conduction band offset between the ETL and the perovskite and VBO is the valence band offset between the perovskite and the HTL. The other parameter that can affect the performance of the PSC is known as the total recombination rate ($\boldsymbol{R''}$) related to the trap density and is given by:

$$\boldsymbol{R''} = \boldsymbol{R_b} + \boldsymbol{R_{SRH}^{Bulk}} + \boldsymbol{R_{SRH}^{\frac{ETL}{Perovskite}}} + \boldsymbol{R_{SRH}^{\frac{Perovskite}{HTM}}} \quad (2)$$

R_b is the band-to-band recombination rate, and R_{SRH} is the Shockley-Redd-Hall trap-assisted recombination. In this study, we will considered the above-described all the sources of recombination to design highly efficient lead-free PSCs.

Table 1. Parameters Used in the SCAPS Simulation of lead-free all-inorganic PSCs.

Parameter	FTO	PCBM[40]	CeO_X	IL1	$CsSn_{0.5}Ge_{0.5}I_3$[20]	IL2	SpiroOMeTAD	PTAA[39]
thickness (nm)	400	90	90	10	Wide range	10	150	150
E_g (eV)	3.5	2	3.5[41]	1.5	1.5	1.5	3.06	2.95
X	4	4	4[41]	3.9	1.5	3.9	2.05	2.3
Ɛr	30	3.9	23[42]	28	28	28	3	3.5
N_c (1/cm³)	2.2×10^{18}	2.2×10^{18}	2.2×10^{18}	2.2×10^{18}	2.2×10^{18}	2.2×10^{18}	2.2×10^{18}	2.5×10^{18}
N_v (1/cm³)	1.8×10^{19}	1.8×10^{19}	1.8×10^{19}	1.8×10^{19}	1.8×10^{19}	2.5×10^{19}	1.8×10^{19}	1.8×10^{19}
μ_n(cm²/Vs)	20	1×10^{-2}	3.692×10^{7}[43]	6	9.47×10^{2}	6	0.0002[44]	1×10^{-4}
μ_p(cm²/Vs)	10	1×10^{-2}	3.692×10^{-7}	6	2.13×10^{2}	6	0.0002	1×10^{-4}
N_A (1/cm³)	--	-	-	-	-	-	-	1×10^{18}
N_D (1/cm³)	2×10^{19}	1×10^{16}	1×10^{20}	1×10^{13}	1×10^{13}	1×10^{13}	1×10^{18}	-
N_t(1/cm³)	1×10^{15}	1×10^{15}	1×10^{15}	Wide range	Wide range	Wide range	1×10^{15}	1×10^{15}

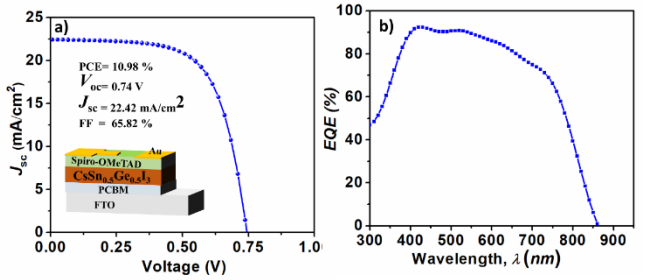

Fig.1. *J-V* characteristics of $CsSn_{0.5}Ge_{0.5}I_3$ perovskite solar cells from the Drift-diffusion simulation.

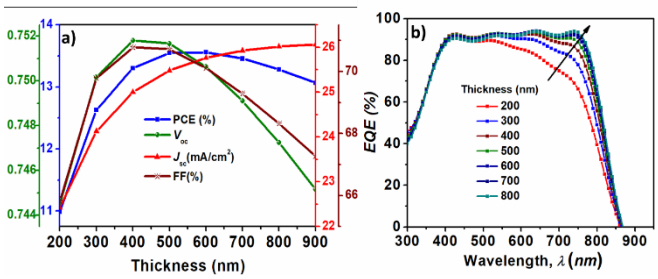

Fig.2. a) The influence of $CsSn_{0.5}Ge_{0.5}I_3$ thickness on the photovoltaics parameters and b) external quantum efficiency (EQE).

3.1 Effect of perovskite layer thickness

The figure of merit in a solar cell is derived by the parameters, namely the open-circuit voltage (V_{oc}), short circuit current density (J_{sc}), and fill factor (FF). Hence, maximizing the value of each parameter is key to achieve high efficiency. The absorber layer thickness significantly influences the microstructure and electro-optical properties as well as the rate of generation and separation of free charges. The best efficiency reported using $CsSn_{0.5}Ge_{0.5}I_3$ displays a thickness of 200 nm,[20] we adapted the value to compute our first model. We investigated the effect of absorber layer thickness on the PV parameters to unravel the optimum value.

Fig.2, illustrates the computed results for the influence of absorber layer thickness (100−900 nm) on PV parameters and external quantum efficiency. The thickness increase in $CsSn_{0.5}Ge_{0.5}I_3$ led to enhancement in PV parameters and peak value suggests optimized thickness. We noted an increase in V_{OC} with an increase in the thickness up to 400 nm. The V_{OC} can be presented by the equation (4) where $\boldsymbol{n}$ is diode ideality factor, $\boldsymbol{Io}$ is dark saturation current, $\boldsymbol{I_L}$ is light-generated current, and $\frac{\boldsymbol{nKT}}{\boldsymbol{q}}$ is thermal voltage:

$$\boldsymbol{V_{oc} = \left({}^{nK_BT}/_{q}\right) ln\left({}^{I_L}/_{Io} + 1\right)} \quad (4)$$

A thicker absorber layer increases the carrier's recombination, therefor I_0 increases more than I_L. After a specific value as suggested above, on further light absorption and an excess carrier concentration, enhances the current density J_{sc} over the range of absorber layer thickness. The maximum PCE attained at 500 nm is 13.57 %, arguably, it can be considered as an optimum thickness to fabricate efficient PSCs as compared to the reported 200 nm. The drop in performance for the thickness >500 nm is due to the higher

chances of recombination in the bulk of perovskites, and the impede movement of free charges.

3.2 Alternative ETLs and HTLs

The energy level aligning between the interlayers as well as the stability of selective layers in the PSCs architect is a key to minimize the energy loss.[37,39] Using CeO_x as an ETL can be an effective path to improve the performance in lead-free PSCs. Firstly (Fig.3a), by employing the CeO_x as an ETL the FF improved, which suggests a favorable interface. The CeO_x possesses attractive optoelectronic properties and low-temperature processing will enhance the stability.[24] The chemical instability and energy level mismatch of Spiro-OMeTAD is an additional challenge for-lead free PSCs development. The VBO is a parameter to measure the energy level between the perovskite layer and HTL. We have demonstrated that reducing the VBO will help to improve the V_{oc} in PSCs [39]. Thus, we have employed PTAA (-5.25 eV) as an HTL, it has a deep energy level compared to the perovskite layer (-5.4 eV) in contrast with Spiro-OMeTAD (-5.11 eV) as shown (Fig. 3b).

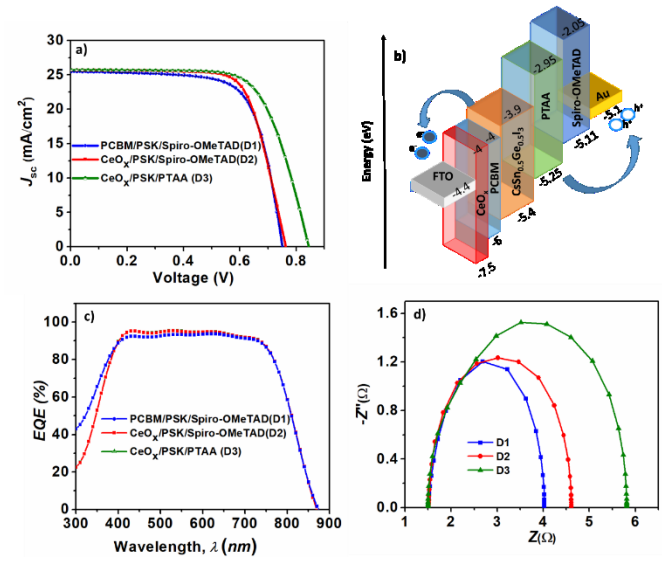

Fig.3. a) *J-V* curves, b) energy level, c), EQE and d) Nyquist plot with different selective layers.

Substitution of the Spiro-OMeTAD with PTAA will reduce the migration distance of holes toward the back contact; subsequently, performance enhancement can be achieved; PCE~15.01%, V_{oc} = 847 mV, J_{sc}~25.71 mA/cm^2, and FF~69.14%. To understand the influence of selective layers, a Nyquist plot (Fig. 3d) of different configurations was simulated. The arc at the low-frequency region is associated with the recombination resistance (R_{rec}), higher R_{rec} values indicate less recombination and efficient separation of free charges at the interfaces.[45] Therefore, it is evident that moving from D1 to D3 PSCs showed less recombination at the interfaces and an enhancement in carrier concentration, suggesting the decisive role of CeO_x and PTAA for performance enhancement in lead-free PSCs. However, the performance is far from the theoretical limit of $CsSn_{0.5}Ge_{0.5}I_3$, and to unravel this ambiguity we focus to other recombination losses.

3.3 Effect of trap density of $CsSn_{0.5}Ge_{0.5}I_3$

Apart from the selective layers of PSCs, the absorber layer's trap density is a key element to achieve high performance which measures the quality of the perovskite. The reported[20] defect density for $CsSn_{0.5}Ge_{0.5}I_3$ is 1E16 cm^{-3}, which is very high as compared to the value in Pb-based perovskites.

To understand the effect of this subtle parameter on the performance of lead-free PSCs and to elucidate the optimum value for $CsSn_{0.5}Ge_{0.5}I_3$, we studied the impact of defect density (N_t) of the perovskite layer on the performance. As illustrated (Fig.4 a-c), the N_t is varied from 1E16 – 1E10 cm^{-3}, as the decrease in N_t leads to an increase in PV parameters exponentially until 1E13, afterward the performance improved gradually and attain maximum values at N_t =1E11 cm^{-3}, thus yielding a PCE~17.42%, with a V_{oc} = 890 mV, J_{sc}~25.75 mA/cm^2, and FF~75.45%. We define the Shockley-read-hall recombination at the bulk perovskite using the following equation:

$$R_{SRH} = \sigma_{n,p} v_{th} N_t \frac{n_p - {n_i}^2}{n+p+2n_i \cos\left(\frac{E_t - E_i}{KT}\right)} \quad (5)$$

Here, σ_n and σ_p are capture cross-section for electrons and holes, v_{th} is thermal velocity, N_t is defect density, n and p are the concentration of electron and hole, n_i is the intrinsic density, E_i is the intrinsic energy level, E_t is the energy level of the trap defect.

The drop in performance is due to increasing non-radiative recombination (Fig. 4 b & d), to have the vice-versa effect, the bulk perovskite layer should be neutralized from defect sites. Decreasing the N_t of bulk perovskite layer (Fig. 4 b, c), reduces the recombination rate by enhancing the lifetime of free charge carriers inside the PSC, thus increase the probability of the collection of free charges at the bottom and front of the PSC. The diffusion length of electrons and holes (Fig. 4c) is calculated by the following equations:

$$L = \sqrt{D\tau}\ (6),\quad \tau_{n,p} = \frac{1}{\sigma_{n,p}\vartheta_{th}N_t}\ (7),\quad D = \frac{\mu T K_B}{q}\ (8)$$

Here L is the diffusion length, $\tau_{n,p}$, the charge carrier lifetime, and D is the diffusion coefficient. K_B and μ represent Boltzmann constant and charge carrier mobility, q and T represent the magnitude of charge and temperature in Kelvin, respectively.

The ideality factor (n) is calculated (Fig. 4e), following equation 4 as described in section 3.1 according to the relationship between the ln (light intensity) versus V_{oc} profile, from the slop $K_B T/q$,

the n showed values >2 which indicates the dominant nature of both bulk SRH and interfaces recombination in the PSCs. With a reduction in the defect density, the n values started to approach 2 and saturated at N_t = 1E12 cm^{-3} with n = 2.51. Furthermore, Fig.4f illustrates the power law depends

between the J_{sc} and the light intensity ($J \propto I^{\alpha}$). Both, the PSCs with high and reduced defect density show a similar slope (α = 0.99) in a double-logarithmic scale, that implying the charge-collection efficiency is independent of light intensity.[46,47]

To minimize the trap vacancy from the bulk perovskite layer, an approach is to use a doping mechanism with different elements or a combination of layered (2D) and 3D perovskites can be an alternative solution. To overcome the challenge of lead-free PSCs, it is paramount to find a suitable fabrication process as an alternative to spin coating processes, as the spin coating process has a high rate of producing pinholes in the presence of Sn^{+4} and Ge^{+4}. Fabrication of lead-free-perovskite with high quality is a demanding task. Based on the results, our PSCs performance is saturated after N_t =1E11 cm^{-3}, we ascribed this to the high trap density at the interfaces of the perovskite layer. To validate our hypothesis, we will highlight the effect of trap density at ETL/perovskite and perovskite/HTL interface.

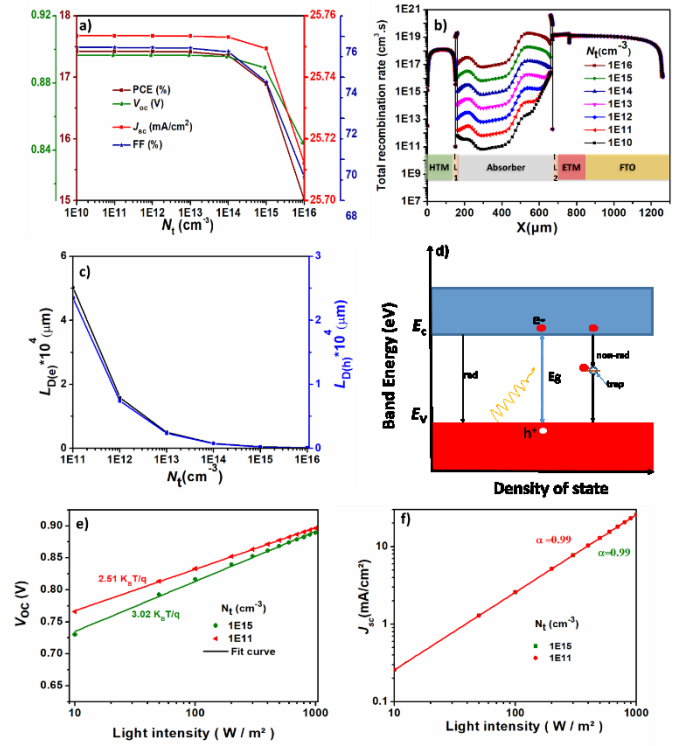

Fig.4. a) Defect density influence on the photovoltaic parameters, b) total recombination rate, c) diffusion length of electrons (black line) and holes (blue line), d) band energy of a perovskite layer, light intensity dependence on, e) V_{oc} and f) $J_{sc.}$

3.4 Interfaces trap density

To understand the interfaces recombination, a modified Shockley-read-hall model that explains the effect of defect density is used [48,49]:

$$R_{IL} = \frac{n_{IL}\, p_{IL} - {n_i}^2}{S_n^{-1}(n_{IL}+n)+S_p^{-1}(p_{IL}+p)} \qquad (9)$$

R_{IL} is the total interface recombination, where (n_{IL}, p_{IL}) are the electron and hole concentration at interfaces. The terms *n* and *p* are related to emission rate from defect energy state to the corresponding band edges (*Ec*, *Ev*) at interfaces. S_n, S_p are the hole and electron interface recombination velocities which are related to the defect density (N_t), capture cross-area of trap for electron as well as hole and the thermal velocity following the equation (9):

$$S_{n,p} = N_t \sigma_{n,p} v_{th} \ (10)$$

For highly doped selective layers, the interface recombination rate reduces to $\boldsymbol{R_{IL} = S_p}$

Arguably, the interfaces are a source of instability and poor performance in the solar cells. Following the above equations, the interface recombination is sensitive to the rate of the trap density. PSCs are fabricated with selective layers which increases the chance of forming defects at the interfaces. Therefore, the effect of defect density at the ETL/Perovskite (IL1) and the Perovskite/HTL (IL2) on the performance of lead free-PSCs was investigated, where thermal velocity and trap capture cross-area for electron and holes are kept constant (Fig. 4).

Remarkably, we noted that defect density at the interfaces impacts the performance of PSCs, particularly the PCE, V_{OC}, and FF. Reducing the defect density at both the interfaces leads to enhancement in the PV parameters. (Fig. 4) Increment in PCE from 17% to over 24 % and similarly the V_{oc} increases from 890 to 1170 mV, and the FF improved from 75 to over 80 %, but with minute gains in the J_{sc} due to injection of free charges remains similar. The red area represents the highest values that can be attained for each PV parameter, thus to achieve this value (Fig. 4), an arrangement of defect density at both interfaces is a prerequisite (Table 2). Additionally, we also noted at the interface, the defect density at the perovskite/HTL is sensitive to the performance and influence the PV properties; by keeping the N_{tIL2} =1E18 cm^{-3} and varied the N_{tIL1}, we noticed the performance remains constant and the blue area (low performance) is dominated. In contrast, when we reduce the N_{tIL2}, the effect of defect density at the ETL/perovskite is observed, conversely to the effect of defect density at the perovskite/HTL, reducing the N_{tIL2} even if the N_{tIL1} is high, the performance of the PSC is boosted from the blue area to the green (Fig. 4). This is supported by the hypothesis that the light first strike through the perovskite/HTL, thus reducing the trap density at the front interface could help the absorber layer to harvest maximum solar radiations by minimizing the recombination channels. Thus, designing high performance, low value of N_{tIL2} is recommended. The defect density at the N_{tIL2} impacts the performance of the PSCs largely and can be an approach to catalyze the effect of defect density at the ETL/Perovskite interface.

Table 2. The arrangement of N_{tIL1} and N_{tIL2} for the red area in Fig.4.

	PCE	V_{oc}	FF	J_{sc}
N_{tIL1}	<1E16	<1E16	<1E16	<1E16
N_{tIL2}	<1E14	<3E14	<2E13	<1E18

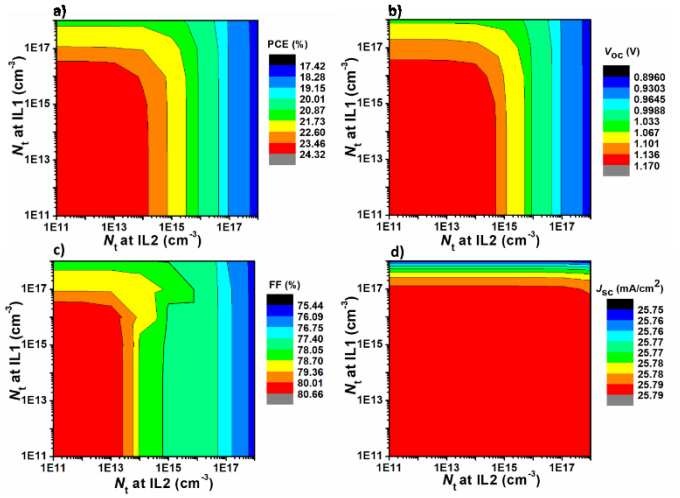

Fig.4. a) The effect of defect density at the Perovskite/ETL (IL1) and Perovskite/HTL (IL2) on the PCE, b) V_{oc} c) FF, and d) J_{sc} of lead-free PSCs based on $CsSn_{0.5}Ge_{0.5}I_3$.

Experimentally, such defect densities value at interfaces could be achieved, by the passivation mechanism especially at the perovskite/HTL interface to suppress the defects. The interface interaction mechanism and with additives for the perovskite layer needs to be studied. The bulk and interfaces are essential to research, to push the performance of lead-free PSCs near to the Pb-based PSCs. To reduce the recombination rate at interfaces, improving the mobility of free charge carriers of selective layers as well as the use of efficient passivating materials that can reduce the interface carrier density and surface recombination velocities is essential. Furthermore, efficient fabrication methods such as thermal co-evaporation, printing, or large-scale industrial technologies [50–52] can help to control the defect density inside the perovskite layer. To benchmark this, we tabulated (Table 3), recent progress in all-inorganic lead-free PSCs with our optimized results, by reducing the discussed different recombination channels.

Table 3. Recent lead-free PSCs summary of experimental (E) and simulation (S) studies.

Perovskite	Method	PCE (%)	V_{oc} (mV)	FF (%)	J_{sc} (mA/cm^2)
$CsSnI_2Br$ [53]	E	1.67	290	38	15.06
{en}$CsSnI_3$ [54]	E	3.79	280	54	25.07
$CsSn_{0.5}Ge_{0.5}I_3$ [20]	E	7.11	630	61	18.61
$CsSn_{0.6}Ge_{0.4}I_3$ [55]	E	4.9	650	64	11.8
$CsSnIBr_2$ [39]	S	20.32	1350	74.17	20.30
$CsSn_{0.5}Ge_{0.5}I_3$	this work	24.20	1170	80.33	25.80

4. Conclusions

In summary, we carried out a computational approach using solar cell capacitance simulator software to unravel the road map for performance enhancement in a lead-free perovskite solar cell based on $CsSn_{0.5}Ge_{0.5}I_3$. We noted an optimized thickness of 500 nm in a configuration of FTO/PCBM/$CsSn_{0.5}Ge_{0.5}I_3$/Spiro-OMeTAD/Au, to be the optimum value while using CeO_x and PTAA further enhances the performance as electron and hole selective layers respectively. The optimized value of the trap density in the bulk of $CsSn_{0.5}Ge_{0.5}I_3$ is found to be ~1E11 cm^{-3}, derived from high-quality perovskites that can decrease the total recombination rate. We conclude that reducing the trap density at perovskite interfaces beyond 1E14 cm^{-3} is the key to boost the performance of Sn-Ge-based PSCs. Furthermore, we observed that the benefit of interface passivation at the perovskite/hole selective interface is higher than that of the electron selective layer/perovskite. This in turn controls the performance improvements in lead-free-PSCs based on $CsSn_{0.5}Ge_{0.5}I_3$.

Conflicts of interest

There are no conflicts to declare.

Acknowledgments

This work has received funding from the European Union H2020 program under the European Research Council Consolidator grant MOLEMAT (726360) and PARASOL (RTI2018-102292-B-100), the Spanish Ministry of Science and Innovation. The authors would like to thank Professor Marc Burgelman, Department of Electronics and Information Systems, the University of Gent for the development of the SCAPS software package and for allowing its use.

References

1 A. Miyata, A. Mitioglu, P. Plochocka, O. Portugall, J. Tse, W. Wang, S. D. Stranks, H. J. Snaith and R. J. Nicholas, *Nat. Phys.*, 2015, **11**, 582–587.

2 T. Leijtens, S. D. Stranks, G. E. Eperon, R. Lindblad, E. M. J Johansson, I. J. McPherson, H. kan Rensmo, J. M. Ball, M. M. Lee, and H. J. Snaith, *ACS Nano*, 2014, **8**, 7147–7155.

3 Y. M. Wang, S. Bai, L. Cheng, N. N. Wang, J. P. Wang, F. Gao and W. Huang, *Adv. Mater.*, 2016, **28**, 4532–4540.

4 N. K. Noel, S. D. Stranks, A. Abate, C. Wehrenfennig, S.

Guarnera, A. A. Haghighirad, A. Sadhanala, G. E. Eperon, S. K. Pathak, M. B. Johnston, A. Petrozza, L. M. Herz and H. J. Snaith, *Energy Environ. Sci.*, 2014, **7**, 3061–3068.

5 F. Li, C. Zhang, J. Huang, H. Fan, H. Wang, P. Wang, C. Zhan, C. Liu, X. Li, L. Yang, Y. Song and K. Jiang, *Angew. Chemie Int. Ed.*, 2019, **58**, 6688–6692.

6 M. Liao, B. Yu, Z. Jin, W. Chen, Y. Zhu, X. Zhang, W. Yao, T. Duan, I. Djerdj and Z. He, *ChemSusChem*, 2019, **12**, 5007–5014.

7 X. Meng, J. Lin, X. Liu, X. He, Y. Wang, T. Noda, T. Wu, X. Yang and L. Han, *Adv. Mater.*, 2019, **31**, 1903721.

8 S. Li, P. Liu, L. Pan, W. Li, S. E. Yang, Z. Shi, H. Guo, T. Xia, S. Zhang and Y. Chen, *Sol. Energy Mater. Sol. Cells*, 2019, **199**, 75–82.

9 C. H. Ng, K. Nishimura, N. Ito, K. Hamada, D. Hirotani, Z. Wang, F. Yang, S. Likubo, Q. Shen, K. Yoshino, T. Minemoto and S. Hayase, *Nano Energy*, 2019, **58**, 130–137.

10 T. Leijtens, G. E. Eperon, N. K. Noel, S. N. Habisreutinger, A. Petrozza and H. J. Snaith, *Adv. Energy Mater.*, 2015, **5**, 1500963.

11 Y. Zhou, H. F. Garces, B. S. Senturk, A. L. Ortiz and N. P. Padture, *Mater. Lett.*, 2013, **110**, 127–129.

12 I. Chung, J. H. Song, J. Im, J. Androulakis, C. D. Malliakas, H. Li, A. J. Freeman, J. T. Kenney and M. G. Kanatzidis, *J. Am. Chem. Soc.*, 2012, **134**, 8579–8587.

13 S. Rühle, *Sol. Energy*, 2016, **130**, 139–147.

14 N. Wang, Y. Zhou, M.-G. Ju, H. F. Garces, T. Ding, S. Pang, X. C. Zeng, N. P. Padture and X. W. Sun, *Adv. Energy Mater.*, 2016, **6**, 1601130.

15 T. Bin Song, T. Yokoyama, S. Aramaki and M. G. Kanatzidis, *ACS Energy Lett.*, 2017, **2**, 897–903.

16 P. Zhu, C. Chen, S. Gu, R. Lin and J. Zhu, *Sol. RRL*, 2018, **2**, 1700224.

17 K. P. Marshall, M. Walker, R. I. Walton and R. A. Hatton, *Nat. Energy*, 2016, **1**, 16178.

18 Q. Tai, X. Guo, G. Tang, P. You, T. W. Ng, D. Shen, J. Cao, C. K. Liu, N. Wang, Y. Zhu, C. S. Lee and F. Yan, *Angew. Chemie - Int. Ed.*, 2019, **58**, 806–810.

19 T. Bin Song, T. Yokoyama, J. Logsdon, M. R. Wasielewski, S. Aramaki and M. G. Kanatzidis, *ACS Appl. Energy Mater.*, 2018, **1**, 4221–4226.

20 M. Chen, M.-G. Ju, H. F. Garces, A. D. Carl, L. K. Ono, Z. Hawash, Y. Zhang, T. Shen, Y. Qi, R. L. Grimm, D. Pacifici, X. C. Zeng, Y. Zhou and N. P. Padture, *Nat. Commun.*, 2019, **10**, 16.

21 Q. K. Wang, R. Bin Wang, P. F. Shen, C. Li, Y. Q. Li, L. J. Liu, S. Duhm and J. X. Tang, *Adv. Mater. Interfaces*, 2015, **2**, 1400528.

22 X. Wang, J. Wu, Y. Yang, X. Liu, Q. Guo, Z. Song, G. Li, Z. Lan and M. Huang, *J. Mater. Chem. A*, 2019, **7**, 13256–13264.

23 X. Wang, L. L. Deng, L. Y. Wang, S. M. Dai, Z. Xing, X. X. Zhan, X. Z. Lu, S. Y. Xie, R. Bin Huang and L. S. Zheng, *J. Mater. Chem. A*, 2017, **5**, 1706–1712.

24 R. Meng, X. Feng, Y. Yang, X. Lv, J. Cao and Y. Tang, *ACS Appl. Mater. Interfaces*, 2019, **11**, 13273–13278.

25 X. Zhang, L. Su, Y. Kong, D. Ma, Y. Ran, S. Peng, L. Wang and Y. Wang, *J. Phys. Chem. Solids*, 2020, **147**, 109651.

26 W. Dong, T. Zhang, X. Chen, B. Wang and B. Zhu, *Phys. status solidi*, 2017, **214**, 1700089.

27 Z. C. Orel and B. Orel, *Phys. status solidi*, 1994, **186**, K33–K36.

28 T. Inoue, M. Osonoe, H. Tohda, M. Hiramatsu, Y. Yamamoto, A. Yamanaka and T. Nakayama, *J. Appl. Phys.*, 1991, **69**, 8313–8315.

29 W. S. Yang, J. H. Noh, N. J. Jeon, Y. C. Kim, S. Ryu, J. Seo and S. Il Seok, *Science*, 2015, **348**, 1234–1237.

30 N. J. Jeon, H. Noh, W. S. Yang, Y. C. Kim, S. Ryu, J. Seo and S. Il Seok, *Nature, 2015, **517**, 476–480*.

31 C. Wehrenfennig, G. E. Eperon, M. B. Johnston, H. J. Snaith and L. M. Herz, *Adv. Mater.*, 2014, **26**, 1584–1589.

32 S. Ravishankar, S. Gharibzadeh, C. Roldán-Carmona, G. Grancini, Y. Lee, M. Ralaiarisoa, A. M. Asiri, N. Koch, J. Bisquert and M. K. Nazeeruddin, *Joule*, 2018, **2**, 788–798.

33 Z. Ni, C. Bao, Y. Liu, Q. Jiang, W.-Q. Wu, S. Chen, X. Dai, B. Chen, B. Hartweg, Z. Yu, Z. Holman and J. Huang, Science,2020, 367, 1352–1358.

34 T. S. Sherkar, C. Momblona, L. Gil-Escrig, J. Ávila, M. Sessolo, H. J. Bolink and L. J. A. Koster, *ACS Energy Lett.*, 2017, **2**, 1214–1222.

35 V. Pecunia, L. G. Occhipinti, A. Chakraborty, Y. Pan and Y. Peng, *APL Mater.*, 2020, **8**, 100901.

36 Y. Peng, T. N. Huq, J. Mei, L. Portilla, R. A. Jagt, L. G. Occhipinti, J. L. MacManus-Driscoll, R. L. Z. Hoye and V. Pecunia, *Adv. Energy Mater.,* 2021, **11**, 2002761.

37 Y. Raoui, H. Ez-Zahraouy, N. Tahiri, O. El Bounagui, S. Ahmad and S. Kazim, *Sol. Energy*, 2019, **193**, 948–955.

38 Y. Raoui, H. Ez-Zahraouy, S. Kazim and S. Ahmad, *J. Energy Chem.*, 2021, **54**, 822–829.

39 Y. Raoui, H. Ez-Zahraouy, S. Ahmad and S. Kazim, *Sustain. Energy Fuels*, 2021, **5**, 219–229.

40 P. Zhao, Z. Liu, Z. Lin, D. Chen, J. Su, C. Zhang, J. Zhang, J. Chang and Y. Hao, *Sol. Energy*, 2018, **169**, 11–18.

41 X. Wang, L. L. Deng, L. Y. Wang, S. M. Dai, Z. Xing, X. X. Zhan, X. Z. Lu, S. Y. Xie, R. Bin Huang and L. S. Zheng, *J. Mater. Chem. A*, 2017, **5**, 1706–1712.

42 F. Chiu and C. Lai, *J. Phys. D: Appl. Phys.*,2010, **43**, 075104.

43 H. L. Tuller and A. S. Nowick, *J. Phys. Chem. Solids*, 1977, **38**, 859–867.

44 T. Minemoto and M. Murata, *J. Appl. Phys.*, 2014, **116**, 054505.

45 C. Wang, H. Hao, S. Chen, K. Cao, H. Yu, Q. Zhang, G. Wan, W. Shang and W. Huang, *RSC Adv.*, 2017, **7**, 29944–29952.

46 J.-W. Lee, D.-H. Kim, H.-S. Kim, S.-W. Seo, S. M. Cho and N.-G. Park, *Adv. Energy Mater.*, 2015, **5**, 1501310.

47 D. Zhao, W. Ke, C. R. Grice, A. J. Cimaroli, X. Tan, M. Yang, R. W. Collins, H. Zhang, K. Zhu and Y. Yan, *Nano Energy*, 2016, **19**, 88–97.

48 H. Wilhelm, H. W. Schock and R. Scheer, *J. Appl. Phys.*, 2011, **109**, 084514.

49 K. W. Kemp, A. J. Labelle, S. M. Thon, A. H. Ip, I. J. Kramer, S. Hoogland and E. H. Sargent, *Adv. Energy Mater.*, 2013, **3**, 917–922.

50 H. A. Dewi, J. Li, H. Wang, B. Chaudhary, N. Mathews, S. Mhaisalkar and A. Bruno, *Adv. Funct. Mater.*, 2021, 2100557.

51 G. Qu, J. J. Kwok and Y. Diao, *Acc. Chem. Res.*, 2016, **49**, 2756–2764.

52 Y. Galagan, Oxford Open Materials Science., 2021, **1**, itaa007.

53 D. Sabba, H. K. Mulmudi, R. R. Prabhakar, T. Krishnamoorthy, T. Baikie, P. P. Boix, S. Mhaisalkar and N. Mathews, *J. Phys. Chem. C*, 2015, **119**, 1763–1767.

54 W. Ke, C. C. Stoumpos, I. Spanopoulos, L. Mao, M. Chen, M. R. Wasielewski and M. G. Kanatzidis, *J. Am. Chem. Soc.*, 2017, **139**, 14800–14806.

55 M. Liu, H. Pasanen, H. Ali-Löytty, A. Hiltunen, K. Lahtonen, S. Qudsia, J. H. Smått, M. Valden, N. V. Tkachenko and P. Vivo, *Angew. Chemie - Int. Ed.*, 2020, **59**, 22117–22125.